

Realizing synergy between Cu, Ga, and Zr for selective CO₂ hydrogenation to methanol



Abdullah J. Al Abdulghani ^a, Edgar E. Turizo-Pinilla ^b, Maria J. Fabregas-Angulo ^b, Ryan H. Hagmann ^c, Faysal Ibrahim ^c, Jacob H. Jansen ^c, Theodore O. Agbi ^a, Samiha Bhat ^d, Miguel Sepúlveda-Pagán ^b, Morgan O. Kraimer ^a, Collin M. Queen ^a, Zhuoran Sun ^c, Eranda Nikolla ^d, Yomaira J. Pagán-Torres ^{b,*}, Ive Hermans ^{a,c,e,**}

^a Department of Chemical and Biological Engineering, University of Wisconsin-Madison, Madison, WI 53706, USA

^b Department of Chemical Engineering, University of Puerto Rico-Mayagüez, Mayagüez, PR 00681, USA

^c Department of Chemistry, University of Wisconsin-Madison, Madison, WI 53706, USA

^d Department of Chemical Engineering, University of Michigan, Ann Arbor, MI 48109, USA

^e Wisconsin Energy Institute, University of Wisconsin-Madison, Madison, WI 53726, USA

ARTICLE INFO

Keywords:
CO₂ hydrogenation
CO₂ utilization
Methanol
Thermocatalysis
Ternary catalysis

ABSTRACT

Hydrogenating CO₂ to methanol with high yields and selectivity remains a kinetic challenge. We report ternary Cu-Ga-Zr catalysts with promising performances. Methanol productivity and selectivity were highest on coprecipitated samples containing approximately 20 wt% of each metal. At 7% isoconversion, this ternary system was more selective to methanol (60 ± 1%) than CuZrO_x (51 ± 1%) and CuGaO_x (53 ± 3%) at the same Cu loading. We uncover the importance of the Cu/Zr interface for CO₂ adsorption, Cu/Ga interface for H adsorption, and metallic Cu for H-H dissociation. Methanol formation on these catalysts was found to be first order in H₂, implying the reaction was likely to be rate-limited by hydrogen activation. In fact, the methanol space-time yield correlated linearly with the H₂/D₂ exchange rate. We propose a catalytic pathway wherein the production of the byproduct CO is hindered by the presence of adsorbed H.

1. Introduction

Process simulations and life cycle assessments have identified the cost of renewable hydrogen as the most critical factor in rendering green methanol from CO₂ economically attractive [1,2]. Recent advances and global initiatives have incentivized the production of hydrogen from renewable energy sources [3–5]. The potential access to low-cost green hydrogen inspires CO₂ hydrogenation as a potential route for the production of green fuels and chemicals from CO₂, including methanol [6–8]. Tuning the activity and selectivity of CO₂ hydrogenation to methanol has been an active area of research with some unresolved questions about the role of the active components [9–14]. The exothermic CO₂ hydrogenation to methanol (CO₂ + 3 H₂ ⇌ CH₃OH + H₂O; ΔH°(25 °C) = -53.3 kJ mol⁻¹) competes with the endothermic CO₂ hydrogenation to CO (*i.e.*, the reverse water gas shift (RWGS) reaction; CO₂ + H₂ ⇌ CO + H₂O; ΔH°(25 °C) = +41.2 kJ mol⁻¹), making

the process less selective at high temperatures [15–17]. Therefore, the development of catalytic systems that promote methanol production and suppress CO production is sought. The industrial methanol production from syngas is catalyzed by a coprecipitated Cu-based catalyst containing Cu, Zn, and Al (Cu/ZnO/Al₂O₃) [9,16,18,19]. Research has proposed that the active site for methanol production is located at the interface between Cu and ZnO [9,18,20,21]. For this catalyst system, Pérez-Ramírez and coworkers have demonstrated that both the CO and CO₂ hydrogenation to methanol scale with the interfacial density of Cu and ZnO in microfabricated catalysts [22]. Attempts have been made to enhance the Cu/oxide interactions by, for example, (partially) substituting ZnO with other metal oxides and introducing additional promoters [23–25].

The ZnO/Al₂O₃ interface in Cu/ZnO/Al₂O₃ has been proposed to be crucial for CO hydrogenation (CO + 2 H₂ ⇌ CH₃OH; ΔH°(25 °C) = -94.5 kJ mol⁻¹) [26,27]. When switching the feed from syngas to just

* Corresponding author.

** Corresponding author at: Department of Chemical and Biological Engineering, University of Wisconsin-Madison, Madison, WI 53706, USA.

E-mail addresses: yomairaj.pagan@upr.edu (Y.J. Pagán-Torres), hermans@chem.wisc.edu (I. Hermans).

CO_2 and H_2 , zirconia has been shown to be a more promising component for methanol production [26]. For CO_2 hydrogenation, the methanol space-time yield (STY) over $\text{Cu}/\text{ZnO}/\text{ZrO}_2$ has been reported to be higher than $\text{Cu}/\text{ZnO}/\text{Al}_2\text{O}_3$ by up to 12% between 220 and 280 °C [28]. Another advantage of ZrO_2 over Al_2O_3 is that ZrO_2 is less hydrophilic, facilitating the desorption of water during CO_2 hydrogenation [29]. The binary Cu/ZrO_2 has also been shown to be more active and selective to methanol than the binary Cu/ZnO [28,30]. The synthesis method and, therefore, the structure of ZrO_2 have been shown to control the reactivity [26,31]. For example, coprecipitated amorphous ZrO_2 is reported to result in more active and selective Cu-based catalysts [26]. The amorphous ZrO_2 has been hypothesized to stabilize small Cu particles and facilitate the desorption of methanol, preventing its decomposition to CO [32,33]. Copéret and coworkers have shown that Cu-Zr/SiO_2 prepared by controlled surface organometallic chemistry exhibits comparable catalytic activity to Cu/ZrO_2 , suggesting that only the interfacial sites are required to enhance methanol activity and selectivity [34,35]. The acid sites at the Cu/Zr interface have been hypothesized to stabilize formates and methoxy intermediates during CO_2 hydrogenation to methanol [36,37].

Another promoter that has been added to Cu-based catalysts is Ga_2O_3 . Incorporating Ga_2O_3 into $\text{Cu}/\text{ZnO}/\text{ZrO}_2$ is hypothesized to result in enhanced Cu reducibility, dispersion, and stabilization of Cu^+ species [38,39]. Huang and coworkers have shown that these promotional effects are also present in the binary $\text{Cu}/\text{Ga}_2\text{O}_3$ [39]. The $\text{Cu}/\text{Ga}_2\text{O}_3$ shows an increase in weak basic sites and a decrease in strong basic sites when compared to the binary $\text{Cu}/\text{Al}_2\text{O}_3$, which has been correlated with the increase in methanol selectivity from 2% to 40% at $T = 250$ °C, $P = 25$ bar, $\text{H}_2/\text{CO}_2 = 4$, and CO_2 conversions between 15% and 18% [39]. The Ga promotional effect has also been reported in Cu/SiO_2 , Cu/ZrO_2 and Pd-based catalysts [40–44]. Baltanás and coworkers have shown that the addition of Ga_2O_3 to Cu/ZrO_2 improves H_2/D_2 exchange rates [40]. Cu-Ga alloys, Ga_x islands, and CuGa_2O_4 nanospinels have been reported and proposed as active sites [43,45–47]. Wu and coworkers reported an increase in oxygen vacancy concentration in GaZrO_x relative to $(\text{Ga}_2\text{O}_3 + \text{ZrO}_2)$ admixtures, which helped in the formation of Ga-H bonds and activation of CO_2 to formate [48]. On the other hand, Cu-Ga/SiO_2 prepared by surface organometallic chemistry has been reported to stabilize methoxy intermediates, but not formates [43].

Herein, we consider the interplay between Cu, Ga_2O_3 , and ZrO_2 in CO_2 hydrogenation catalysts. We report the synthesis, characterization, and reactivity of ternary Cu-Ga-Zr catalysts. To investigate the effect of each component and their interactions, the Ga:Zr loading was varied while the Cu loading was fixed at 20 wt%. We seek to rationalize the nature of active sites of these catalysts using different structural characterization tools, probe reactions, and kinetic studies. We propose H_2 activation as the rate-limiting step for methanol production. Our findings suggest that the Cu/Ga interface stabilizes adsorbed H species, which improves the methanol selectivity by hindering CO formation.

2. Experimental

2.1. Catalyst synthesis

The CuGaZrO_x catalysts were synthesized by coprecipitation from the corresponding nitrate solutions. $\text{Cu}(\text{NO}_3)_2 \cdot 3\text{H}_2\text{O}$, $\text{Ga}(\text{NO}_3)_3 \cdot \text{H}_2\text{O}$, and $\text{ZrO}(\text{NO}_3)_2 \cdot \text{H}_2\text{O}$ (masses and purities are provided in Table A.1) were dissolved in 50 mL of deionized water (resistivity of 18.2 MΩ cm). A solution of 10% (w/v) Na_2CO_3 was added dropwise (*ca.* 3 mL min⁻¹) to the mixed nitrate solution while stirred at room temperature until the pH of the solution reached 10.5 (or a pH of 6 for the synthesis of pure Ga_2O_3 to minimize the formation of the soluble Ga(OH)_4^-). The slurry was stirred for an additional hour. The precipitate was recovered by centrifugation (at least 4400 rpm for 15 min) and washed multiple times with deionized water (resistivity of 18.2 MΩ cm) until the pH of the solution was neutral. The recovered powder was dried overnight at 120

°C. Finally, the catalysts were calcined in a muffle furnace under air at 400 °C with a ramp rate of 2 °C min⁻¹ and a hold time of 2 hours. We denote ternary coprecipitated catalysts as $\text{Cu-GaZrO}_x\text{-Z}$ where Z is the percentage of the molar ratio of Zr ($Z = n_{\text{Zr}} / (n_{\text{Cu}} + n_{\text{Ga}} + n_{\text{Zr}})$) in the catalyst as determined by the inductively coupled plasma-optical emission spectroscopy (ICP-OES) measurements.

As a control catalyst, we impregnated Cu onto an amorphous GaZrO_x support using incipient wetness impregnation (IWI) to obtain 20 wt% Cu loading. To synthesize the amorphous support, $\text{Ga}(\text{NO}_3)_3 \cdot \text{H}_2\text{O}$ was dissolved in 100 mL ethanol and stirred continuously overnight. Then, 16 aliquots of 100 μL each of NH_4OH were added to the solution, 10 minutes apart while stirring. The turbid solution was aged for an additional hour at room temperature. Next, 0.8 mL of $\text{Zr}(\text{OC}_3\text{H}_7)_4$ was added dropwise to the solution followed by the rapid addition of 1 mL of deionized water (resistivity of 18.2 MΩ cm). The reaction was left to proceed for 24 hours. Finally, the solution was heated under stirring at 80 °C until the evaporation of the solvent was achieved. The powder was crushed and calcined under air at 400 °C with a ramp rate of 2 °C min⁻¹ and a hold time of 2 hours. After impregnating the support with Cu via IWI, the sample was recalcined using the same calcination protocol. We denote the ternary IWI catalyst as $\text{Cu/GaZrO}_x\text{-Z}$ where Z is the percentage of the molar ratio of Zr ($Z = n_{\text{Zr}} / (n_{\text{Cu}} + n_{\text{Ga}} + n_{\text{Zr}})$) in the catalyst as determined by the ICP-OES measurements.

2.2. Kinetic measurements

CO_2 hydrogenation experiments were performed using a homebuilt fixed-bed flow reactor setup. Approximately 150 mg of each sample was pressed and sieved into pellets of size 45–90 μm. The catalyst particles were transferred into the middle of a stainless-steel tube (5.5 mm internal diameter), packed in between quartz chips of size 90–150 μm and quartz wool at both ends. The temperature of the catalyst bed was monitored and controlled using a type K thermocouple connected to a temperature controller (Oaktron Digisense 9500). The catalysts were pretreated in 45 sccm H_2 at 300 °C with a ramp rate of 4 °C min⁻¹ and a hold time of 2 hours. After pretreatment, the reactor was purged with N_2 and pressurized to 35 bar. The temperature was then lowered to 220–280 °C for CO_2 hydrogenation testing. A reactor feed mixture of $\text{H}_2/\text{CO}_2/\text{N}_2$ at an 8/2/1 ratio (where N_2 was utilized as an internal standard) was introduced using mass flow controllers (Brookes Instrument SLA5800). The inlet flowrate was set to match the desired weight hourly space velocity (WHSV), typically between 24,000 and 48,000 mL (STP) g_{cat}⁻¹ h⁻¹. The reactor effluent was transferred in a heated line, preventing condensation of products, to an online gas chromatograph (Shimadzu GC-2014) equipped with multiple injection ports. For the quantification of CO_2 , CO, and N_2 , the reactor effluent was injected to the Shimadzu GC-2014 inlet equipped with Hayesep-T (80/100 mesh), Hayesep-Q (80/100 mesh), MSieve 5A (60/80 mesh), and Hayesep-D (80/100 mesh) columns interfaced with a thermal conductivity detector (TCD) and flame ionization detector (FID) with methanizer. For quantification of CH_3OH and dimethyl ether, the reactor effluent was analyzed in the Shimadzu GC-2014 injection port equipped with an RTx-1701 (30 m x 0.32 mm ID) column and FID. The GC response factors for the various species were determined using gas mixtures within a range of known concentrations. The outlet CO_2 , CH_3OH , CO, and dimethyl ether were all quantified with a carbon balance of ≥ 98%.

2.3. Structural characterization

X-ray diffraction (XRD), ICP-OES, and N_2 Brunauer–Emmett–Teller (BET) analyses were performed on the samples to determine their structures, compositions, and specific surface areas, respectively. XRD patterns were obtained using a Bruker D8 Advance diffractometer from 20 of 20° to 80° in 0.1° increments, each with an exposure time of 2 seconds. The ICP-OES experiments were performed using Agilent 5110. Approximately 30 mg of each sample were digested in 10 mL of

2:1 (v/v) H₂SO₄:H₂O (resistivity of 18.2 MΩ cm) for at least 24 hours under stirring and heating (*ca.* 120 °C) with reflux. The BET analysis was based on the physisorption of N₂ at 77 K, which was performed in Quantachrome NovaTouch LX. X-ray absorption spectroscopy (XAS) was measured at the Advanced Photon Source of Argonne National Laboratory at beamline 12-BM-B. The spectra at the K-edge of Cu (8.98 keV), Ga (10.37 keV), and Zr (18.00 keV) were collected in transmission mode. The CuGaZrO_x samples were mixed in *h*-BN (*ca.* 20 wt% sample), reduced (25% H₂/Ar at 300 °C and 35 bar), and then transferred to an inert glovebox filled with nitrogen. The samples were pressed into 30 μm-thick pellets and mounted in sample holders. The sample holders were covered with Kapton tape before transferring them from the glovebox for XAS analysis. The step size in the X-ray absorption near edge structure (XANES) region was set to 0.1 eV. The step size increased gradually to 5 eV in the extended X-ray absorption fine structure (EXAFS) region. Approximately 15 minutes elapsed per 1 scan.

Fresh samples (*ca.* 20 mg) were reduced for X-ray photoelectron spectroscopy (XPS) and scanning electron microscopy (SEM) with energy dispersive X-ray spectroscopy (EDX) analyses in a flow tube furnace under 100% hydrogen at a ramp rate of 4 °C min⁻¹ and held at 300 °C for 2 hours. Analysis was conducted on the reduced samples loaded into an open XPS sample holder exposed to air prior to loading in the UHV chamber of the XPS instrument. The C 1 s, Cu 2p, Ga 2p, and Zr 3d regions were analyzed by Thermo Scientific XPS equipment with a micro-focused monochromated Al K-alpha X-ray source at 10⁻⁷ mbar pressure (UHV) and near room temperature. A flood gun was used to reduce possible sample charging during analysis. Regions were analyzed using a 50 eV pass energy, a 50 ms dwell time, a 400 μm spot size, and a 0.2 eV or 0.1 eV step size. The number of average scans per region was adjusted to achieve an acceptable signal to noise ratio. The recorded data was referenced to the set of adventitious carbon peaks at 284.8 eV as described elsewhere [49]. Peak fitting and integration for the reported relative elemental compositions and electronic assignments were performed via the Avantage (Thermo Scientific) Software package. Typically, peaks were fitted via 30% Lorentz-Gaussian convolve mix (GL30) using a Powell fitting algorithm to minimize the residual difference between the computed envelope and experimental data. All peaks were fitted using a convolution of Shirley and Tougaard backgrounds. Peak splitting energies and FWHM values, referenced to literature values and the NIST XPS database, were used as constraints in peak assignments. Rigorous quantification of Cu was difficult on samples containing Cu(0), Cu(I), and Cu(II). It has been shown that comparing the relative area of the shake-up peak can be used to quantify the relative value for Cu(0) + Cu(I) : Cu(II) [49–51]. This is due to incomplete relaxation to the ground state for the Cu(II) species responsible for the shake-up peaks. This incomplete relaxation was not observed for Cu(0) or Cu(I). Peak areas in the Cu 2p region were used according to the methodology outlined by Biesinger *et al.* in the determination of Cu(0) + Cu(I) : Cu(II) values [49–51]. SEM/EDX images were collected on a Zeiss 450/LEO 1530 instrument. Samples were prepared on carbon tape using 2 keV for images and 20 or 30 keV for EDX analysis.

HAADF-STEM (high-angle annular dark-field scanning transmission electron microscopy) micrographs were obtained on a 200 kV FEG scanning transmission electron microscope (Thermo Fisher Talos F200X G2) at the MC2 characterization facility at the University of Michigan, Ann Arbor. The Cu-GaZrO_x-24 sample was prepared by crushing and dispersing 1.5 mg of the sample in 2 mL of isopropanol with continuous sonication for an hour. The dispersions were then dropped onto holey carbon coated Cu grids and dried for 2 hours before imaging. The samples were also plasma cleaned using a Gatan Solarus II Plasma Cleaning System to remove any impurities before imaging. EDX mapping of Cu, Ga, and Zr particles at two different spots was obtained by performing continuous elemental scans on one spot for 20 minutes with a dwell time of 10 μs per scan. The elemental mapping was done in a net intensity mode under long scanning rates to suppress background noise from the Cu grid.

2.4. Probe reactions

Temperature programmed reduction (H₂-TPR) and N₂O titration experiments were carried out using a homebuilt setup utilizing SRI 8690 as a TCD of the effluent gases (Fig. A.1). Approximately 100 mg of each sample were packed in a 3/8" outer diameter stainless-steel tube in between quartz wool plugs and quartz chips. The samples were reduced (TPR) in 50 sccm 5% H₂/N₂ and heated to 400 °C with a ramp rate of 5 °C min⁻¹. The temperature was held at 400 °C for 30 minutes under 50 sccm He to flush adsorbed H₂ and the lines. Then, the temperature was lowered to 40 °C for N₂O pulse chemisorption experiments. At this temperature, N₂O oxidizes surface Cu(0) to Cu(I) (2 Cu + N₂O → Cu₂O + N₂), but bulk copper is assumed to be unaffected [52–58]. A 250-μL sample loop was filled with 10% N₂O/He and injected to the samples using pure He as a carrier gas. A total of 100 injections were performed on each sample. The effluent gas passed through a cold trap filled with liquid nitrogen to condense unreacted N₂O [59]. The resulting N₂/He mixture was analyzed using a calibrated TCD. The Cu dispersion (*D*_{Cu}, the amount of surface Cu in a sample as a percentage of its total Cu content) was calculated using the equation:

$$D_{Cu} = \frac{2n_{N_2,N_2O}}{n_{H_2,TPR}}$$

where *n*_{N₂,N₂O is the number of moles of N₂ produced in the N₂O titration step and *n*_{H₂,TPR} is the number of moles of H₂ consumed in the H₂-TPR step.}

Temperature programmed desorption of CO₂ (CO₂-TPD) experiments were carried out using a thermogravimetric analysis-differential scanning calorimetry-mass spectrometry (TGA-DSC-MS) setup. The TGA-DSC was performed on a Mettler Toledo TGA/DSC 1 instrument, the effluent of which was fed into a Pfeiffer Omnistar GSD 320 mass spectrometer. Around 50 mg of each sample were reduced in 30 sccm 4% H₂/N₂ and heated to 300 °C with a ramp rate of 5 °C min⁻¹. The temperature was held at 300 °C for an hour under the reducing conditions before the flowing gas was switched to 30 sccm N₂ for 30 minutes at the same temperature. Then, the temperature was lowered to 25 °C. At 25 °C, CO₂ was fed for 30 minutes and then purged by N₂ for 30 more minutes. The temperature was finally raised to 800 °C with a ramp rate of 10 °C min⁻¹. The desorption of CO₂ was monitored by measuring *m/z* = 44 in the MS. Savitzky-Golay smoothing was applied to the CO₂-TPD profiles.

H₂-TPD and H₂/D₂ exchange experiments were performed in a homebuilt setup utilizing a Pike DiffusIR chamber as a reactor, the effluent of which was monitored by an Extrel MAX300-CAT mass spectrometer. Around 40 mg of each calcined sample were used for either experiment. For H₂-TPD, the samples were reduced in 30 sccm H₂ from 30 °C to 300 °C, with a ramp rate of 10 °C min⁻¹ and a hold time of 30 minutes. The samples were cooled to 30 °C and the flowing gas was switched to 30 sccm Ar for 1 hour. The samples were heated in Ar to 600 °C with a ramp rate of 10 °C min⁻¹. The desorption of H₂ was monitored by measuring *m/z* = 2 in the MS, normalized by the Ar signal as an internal standard. For the H₂/D₂ exchange, the experiments were carried out at 6 bar by a backpressure regulator downstream of the reactor. The samples were reduced from 25 °C to 300 °C under 42 sccm 4.76% H₂/Ar with a ramp rate of 5 °C min⁻¹ and a hold time of 30 minutes. The samples were then cooled to 140 °C. At this temperature, 40 sccm 10% H₂/10% D₂/Ar were fed for at least 20 minutes to reach steady state. Afterwards, the feed composition was changed to 10% H₂/10% D₂/5% CO₂/Ar. The conversion of H₂ and the formation of HD were monitored by measuring *m/z* = 2 and *m/z* = 3, respectively, in the MS, both normalized by the Ar signal as an internal standard.

3. Results and discussion

3.1. CO_2 hydrogenation performance

Fig. 1 and **Table A.2** show the catalytic activity of Cu-GaZrO_x-Z (Z=19, 24, 48, 65) and benchmark catalysts, Cu-ZrO_x and Cu-GaO_x, as space-time yield (STY) instead of turnover frequencies, given that the active sites for these catalysts have not yet been established. The binary GaZrO_x was the least active catalyst (**Fig. 1b**), highlighting that Cu is crucial for converting CO₂. Although the synthesized CuGaZrO_x samples have similar Cu loadings of 20 ± 3 wt% (**Table 1**), different CO₂ hydrogenation activities were observed across the samples, implying that bulk Cu loading is not the sole determining factor for CO₂ hydrogenation reactivity. Cu may synergistically interact with Ga and Zr. The methanol STY was the highest on the ternary Cu-GaZrO_x-24, which outperformed the tested binary systems, Cu-ZrO_x and Cu-GaO_x. Even when the methanol production rate was normalized by the surface area (**Fig. A.2**), the best performing catalyst remained a ternary catalyst (Cu-GaZrO_x-65). From these observations, we conclude that CuO_x, GaO_x, and ZrO_x may interact in a way that boosts the methanol STY. At 260 °C and similar CO₂ conversions of approximately 7% (far from the equilibrium conversion of 25%) obtained by varying the WHSV between 24,000 and 48,000 mL(STP) g_{cat}⁻¹ h⁻¹, the methanol selectivity on the coprecipitated catalysts increased as the Ga content increased, but reached a maximum on the ternaries Cu-GaZrO_x-48 and Cu-GaZrO_x-24 (**Fig. 1b**). These results highlight the ability of Cu-GaZrO_x-24 and Cu-GaZrO_x-48 to produce methanol more efficiently and/or to suppress the RWGS reaction. Cu-GaZrO_x-24 demonstrated a stable time-on-stream performance at 280 °C with a negligible loss in methanol productivity after 24 hours (**Fig. 1c**). **Table A.3** and **Table A.4** demonstrate the absence of extra- and intraparticle mass transfer limitations on the best performing catalyst Cu-GaZrO_x-24. When compared with the industrial Cu/ZnO/Al₂O₃ catalyst at the same WHSV (**Fig. A.3**), Cu-GaZrO_x-24 is a more productive catalyst for methanol synthesis when the rate is normalized by the bulk Cu content (2.7 ± 0.1 g_{MeOH} g_{Cu}⁻¹ h⁻¹ on Cu-GaZrO_x-24 vs 2.4 ± 0.2 g_{MeOH} g_{Cu}⁻¹ h⁻¹ on Cu/ZnO/Al₂O₃). It should be noted that the tested Cu/ZnO/Al₂O₃ catalyst contains 43 Cu wt%, about twice the amount of Cu in Cu-GaZrO_x-24. Cu/ZnO/Al₂O₃ also has a higher amount of accessible surface Cu ($D_{\text{Cu}} = 7.6\%$) as determined by N₂O titration measurements, which means Cu-GaZrO_x-24 is even more remarkable when the rate is normalized by the accessible surface Cu content ($D_{\text{Cu}} = 1.6\%$). In this paper, we aim to rationalize the improved activity of Cu in CuGaZrO_x catalysts and the synergistic interactions between Cu, Ga, and Zr.

3.2. Structure and reducibility

XRD analysis (**Fig. 2a**) indicates that the calcined coprecipitated samples have no detectable crystalline phases. This implies that the samples are either amorphous or consist of small crystalline particles below the XRD detection limit. To produce the Cu(IWI)/GaZrO_x sample, we initially synthesized GaZrO_x using coprecipitation, but the XRD pattern of the calcined sample showed the presence of α -Ga₂O₃ crystalline phase (**Fig. A.4**). Since none of the other coprecipitated samples showed detectable crystalline phases, we decided to use a different synthesis protocol that resulted in an amorphous GaZrO_x phase. Impregnating the amorphous GaZrO_x support with Cu (*i.e.*, to produce the sample Cu/GaZrO_x-19) resulted in a sample that showed CuO XRD signals upon calcination. The Cu/GaZrO_x-19 reactivity was lower than that of the coprecipitated Cu-GaZrO_x-24 (**Fig. 1a**), possibly implying the importance of Cu proximity to the GaO_x and ZrO_x phases. N₂O titration experiments showed that the coprecipitated sample has 2.6 more surface Cu(0) than the IWI analog, which is notably the ratio of their methanol STY. SEM-EDX mapping was performed on the coprecipitated Cu-GaZrO_x-24 and Cu(IWI)/GaZrO_x-19 samples (**Fig. A.5**). The coprecipitated sample showed more homogenous distribution of Cu, particularly the

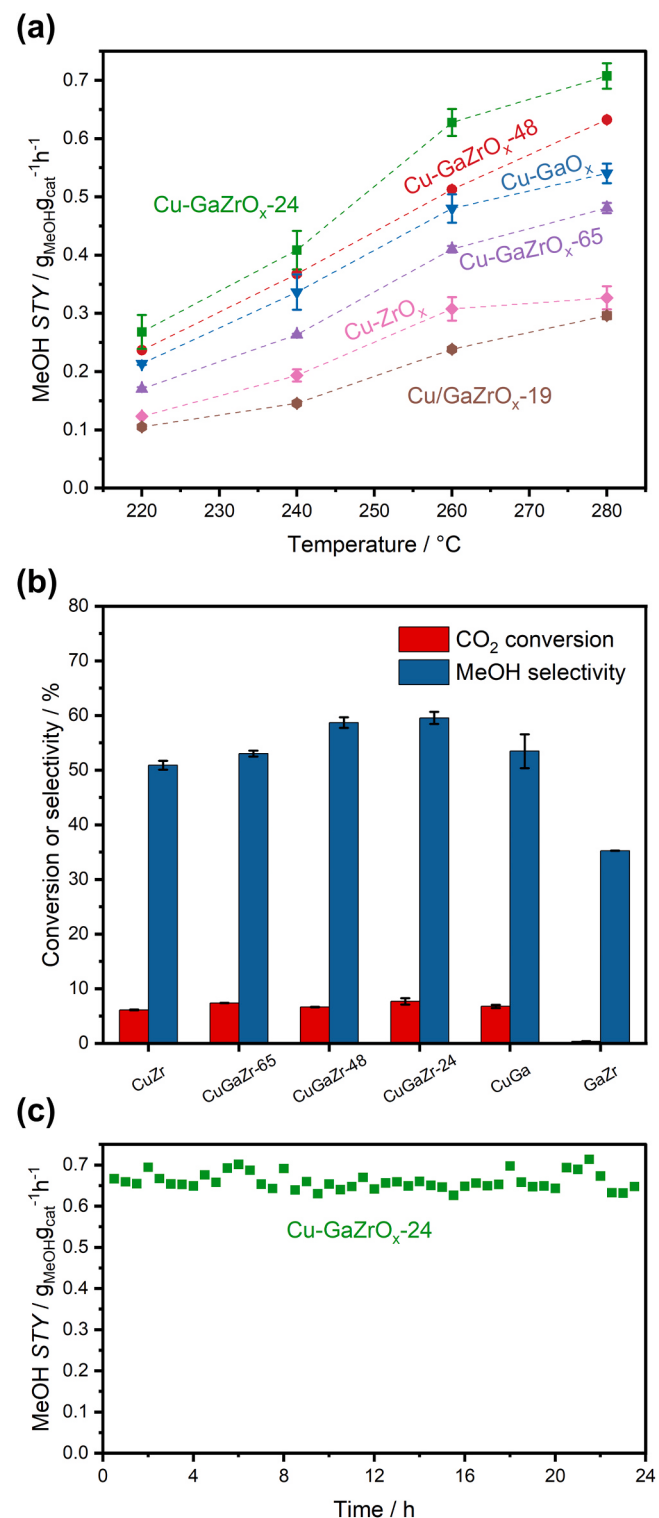


Fig. 1. (a) Methanol space-time yield (STY) as a function of the reaction temperature on CuGaZrO_x samples of different compositions and syntheses at WHSV of 48,000 mL(STP) g_{cat}⁻¹ h⁻¹. (b) CO₂ conversion and methanol selectivity of the coprecipitated CuGaZrO_x samples at 260 °C and WHSV of 48,000 mL (STP) g_{cat}⁻¹ h⁻¹, except for Cu-ZrO_x and CuGaZrO_x-65 where the WHSV was lowered to 24,000 mL(STP) g_{cat}⁻¹ h⁻¹ to achieve higher conversion. (c) Methanol STY as a function of time-on-stream on Cu-GaZrO_x-24 at 280 °C and WHSV of 48,000 mL(STP) g_{cat}⁻¹ h⁻¹. The reactor pressure was 35 bar and inlet H₂/CO₂ ratio was 4/1. Raw data of **Fig. 1a** are provided in **Table A.2**.

Table 1

Metallic loadings, BET surface areas (S_{BET}), and copper dispersion (D_{Cu}) of the CuGaZrO_x samples based on ICP-OES, N₂ physisorption, and N₂O titration measurements, respectively.

Sample ^a	Cu wt%	Ga wt%	Zr wt%	$S_{BET} / \text{m}^2 \text{g}^{-1}$	$D_{Cu} / \%$
Cu-ZrO _x	24	0	47	112	1.0
Cu-GaZrO _x -65	16	4	52	109	1.5
Cu-GaZrO _x -48	19	9	36	166	1.0
Cu-GaZrO _x -24	23	22	20	217	1.6
Cu(IWI)/GaZrO _x -19	17	34	17	85	0.6
Cu-GaO _x	22	45	0	153	3.1

^a The Z in Cu-GaZrO_x-Z refers to the percentage of the molar ratio Zr / (Zr + Cu + Ga).

mixing of Cu with Ga throughout the sample. In contrast, the Cu/GaZrO_x-19 showed more agglomeration of Cu particles, resulting in less dispersion between Cu and Ga relative to the coprecipitated counterpart. Fig. 2c shows the HAADF-STEM-EDX mapping of Cu-GaZrO_x-24, which further confirms the homogenous distribution of Cu, Ga, and Zr.

To study the effect of calcination temperature on the structure and activity, the Cu-GaZrO_x-24 sample was also calcined at temperatures higher than 400 °C, namely at 550 °C and 700 °C. Calcination at both 400 °C and 550 °C resulted in samples with no evidence for crystalline particles according to their XRD patterns (Fig. 2b). However, crystalline CuO, CuGa₂O₄, and *t*-ZrO₂ XRD peaks appeared for the sample calcined at 700 °C. Activity measurements show that the sample calcined at 700 °C exhibited lower methanol STY than the sample calcined at 400 °C (Fig. A.6). This observation suggests that amorphous phases, small particles, and/or interfaces may be co-responsible for the enhanced methanol STY.

H₂-TPR profiles (Fig. 3) show that only Cu-containing samples were reducible below 300 °C (i.e., the standard pretreatment temperature in the reactivity studies). A remarkable difference between the H₂-TPR profiles of the coprecipitated samples and the IWI one is the presence of two reduction peaks, which have been reported previously in the literature and are still under debate. The stepwise reduction from Cu(II) to Cu(I) to Cu(0) is among the proposed explanation of the double peak behavior, especially when Cu is strongly interacting with other metal oxides [60]. Our coprecipitated samples may contain CuO phases that strongly interact with Ga and Zr oxides, stabilizing the stepwise reduction of Cu(II). For the IWI sample, however, the incorporation of Cu occurred on top of the GaZrO_x support, which minimized the interaction of Cu with the other metals, resulting in a H₂-TPR profile that resembles that of bulk CuO (Fig. A.7). Another explanation for the double peak feature is the presence of highly dispersed CuO phases that undergo reduction at a lower temperature than the bulk-like CuO phases [39,61]. Nevertheless, both reduction peaks are below 300 °C, meaning metallic copper is the likely phase of Cu under reaction conditions. At elevated partial pressures of hydrogen, which is the case in reactivity studies, the reductions are expected to occur at even lower temperatures than the temperatures observed in the ambient H₂-TPR profiles. Fig. A.8 shows the XRD patterns of Cu-GaZrO_x-24 calcined, reduced, and after the CO₂ hydrogenation reaction. The XRD patterns of the reduced and spent sample showed metallic Cu peaks. N₂O pulse chemisorption experiments (Fig. A.9) indicate that Cu-GaO_x had the highest amount of surface Cu(0) among the CuGaZrO_x samples, but it was not the one with the highest methanol STY. In fact, considering all the samples together, there seems to be no linear correlation between the methanol STY and the amount of surface Cu(0) as determined by N₂O pulse chemisorption (Fig. A.10). These findings do not necessarily imply some limitations on N₂O titration measurements, but may suggest: i) a dynamic behavior of the catalysts in which the surface density of Cu(0) is different at reaction conditions than the typical conditions of N₂O titrations, ii) the presence of surface Cu(I), which is theoretically inert to N₂O at low temperatures, or Cu(II) species that influence reactivity, iii) the importance of the local

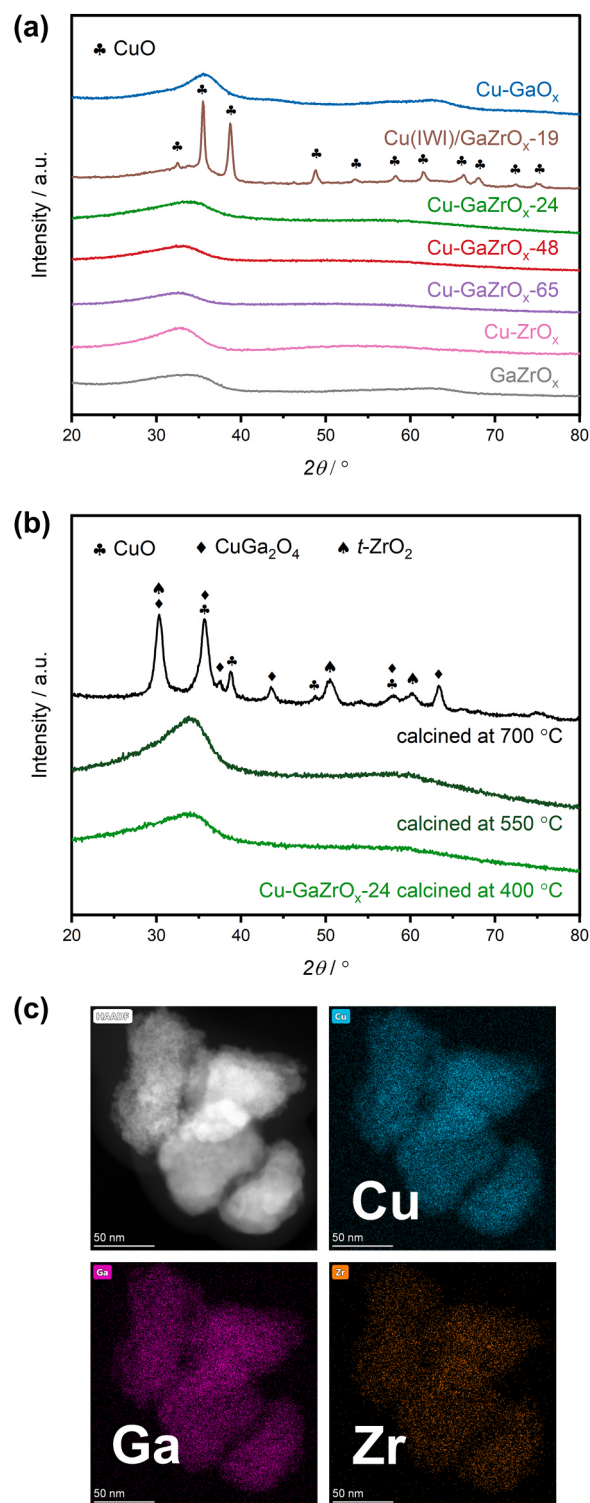


Fig. 2. (a) *Ex-situ* powder XRD patterns of the CuGaZrO_x samples calcined at 400 °C. (b) Effect of calcination temperature on the *ex-situ* powder XRD pattern of Cu-GaZrO_x-24. (c) HAADF-STEM-EDX mapping of Cu-GaZrO_x-24 calcined at 400 °C.

environment of Cu(0) to its activity, or iv) an influence of subsurface Cu on GaO_x and/or ZrO_x reactivity.

The Cu 2p XPS spectra of the reduced samples (Fig. 4a) show unreduced surface Cu species. Cu(II) is clearly present on the coprecipitated samples, as evident by the shake-up feature, whereas the IWI sample is mainly Cu(0/I). We draw attention to the fact that the reduced samples

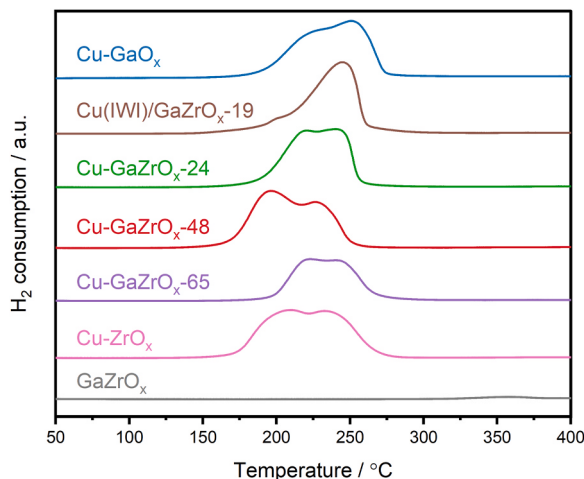


Fig. 3. H₂-TPR profiles of the CuGaZrO_x samples. The samples (100 mg each) were reduced under 50 sccm 5% H₂/N₂ with a ramp rate of 5 °C min⁻¹.

were briefly exposed to air prior to the XPS analysis, which may have caused the oxidation of Cu species. To gauge the extent of ambient oxidation, we performed a TGA-DSC experiment in which Cu-GaZrO_x-24 and GaZrO_x were reduced in 4% H₂/N₂ at 300 °C, cooled in N₂ to 30 °C, exposed to air for 1 hour, and then reduced again at 300 °C. The DSC curve corresponding to the introduction of ambient air over the Cu-GaZrO_x-24 sample (Fig. 4d) shows a sharp exothermic peak. The corresponding TGA curve on that sample shows an abrupt gain in weight followed by a steady increase to a total of 0.9 wt% increase at the 1-hour mark. On the other hand, the TGA-DSC curves of GaZrO_x do not show these features, indicating that Cu is what is oxidized abruptly upon the introduction of air at 30 °C. A weight gain of 0.9 wt% is more than the weight gain caused by the oxidation of surface Cu to CuO, as determined by the following equations:

$$(wt\% \text{ gain after surface oxidation}) = (\text{ICP Cu wt\%})(D_{Cu}) \left(\frac{M_O}{M_{Cu}} \right)$$

$$(wt\% \text{ gain after bulk oxidation}) = (\text{ICP Cu wt\%}) \left(\frac{M_O}{M_{Cu}} \right)$$

where D_{Cu} is the copper dispersion as determined by N₂O titration measurements and M_O and M_{Cu} are the molar masses of O and Cu, respectively. For Cu-GaZrO_x-24, the theoretical weight gains upon surface and bulk oxidation are 0.1 wt% and 5.8 wt%, respectively. Our observed bulk oxidation gain (determined by the difference in mass between the calcined and reduced Cu-GaZrO_x-24 during the TGA experiment) was within 0.2 wt% of the theoretical value, which could serve as a measure of experimental uncertainty in the ICP and TGA measurements. The observed oxidation value of 0.9 wt% by ambient air is still greater than that of the theoretical weight gain (0.1 wt%) upon the oxidation of surface Cu to CuO. This implies that not only the surface of this sample is oxidized after air exposure for 1 hour, but even some of the bulk. Nevertheless, since the samples were treated equally and were exposed to air for the same amount of time, the Cu 2p XPS data (Fig. 4a) shows the susceptibility of the Cu species to oxidation. The Cu in the coprecipitated samples is more oxidizable than the Cu in the IWI sample, which may be another outcome of the coprecipitated Cu species being more intimately mixed with the other metals. The Ga 2p XPS spectra (Fig. 4b) indicate that the surface Ga species in the coprecipitated samples are less oxidized than the surface Ga in the IWI sample, the Ga 2p_{3/2} peak of which closely aligns with the literature value for Ga₂O₃ (1118.1 eV) [62,63]. The XPS peak at the higher binding energy (around 1120 eV) has been attributed to Ga³⁺ hydroxide [64–66]. The Zr 3d XPS spectra show 2 doublets (Fig. 4c), which have been attributed to ZrO₂

and Zr(OH)₄ [67,68]. The ZrO₂ doublet peak position of the coprecipitated samples (especially for the Ga-containing ones) shifted to lower binding energies than that of the IWI sample, which points to the existence of surface Zr in a partially reduced state. The shifts toward lower binding energies in Ga and, to a lesser extent, Zr XPS spectra of the coprecipitated samples relative to pure Ga₂O₃ and ZrO₂ further highlight the intimate mixing of metals.

The reduced samples were also analyzed using *ex-situ* XAS. The Cu K-edge spectra were fitted using linear combinations of Cu, Cu₂O, and CuO standards between 8950 and 9020 eV (Fig. 4e). The Cu-ZrO_x binary showed the highest metallic Cu content among the samples (71% Cu). The Cu percentage decreased as the Ga content increased, dropping to 49% Cu in the binary Cu-GaO_x. These percentages are lower than the ones obtained by XPS, implying that the surface Cu in these samples is more susceptible to oxidation than the bulk. Furthermore, the IWI sample followed the same trend as the other samples, suggesting that there is some mixing of Cu with bulk GaZrO_x in the Cu/GaZrO_x-19 sample, but the extent of mixing at the surface is not pronounced. It should be noted that the *ex-situ* XRD of all reduced samples, which also were exposed to air prior to analysis, did not exhibit distinguishable Cu₂O or CuO XRD peaks (Fig. A.8). Therefore, the Cu oxide species that are observed by XAS are likely part of amorphous phases in the CuGaZrO_x samples. The Ga K-edge (Fig. 4f) further agree with the possible mixing of Cu and Ga in the IWI bulk. The edge energy shifted to a lower value in Cu-containing samples (including Cu/GaZrO_x-19) than that of GaZrO_x or Ga₂O₃. These shifts in edge energies indicate that Ga partial reduction is not only at the surface (XPS), but extends to the bulk (XAS). On the other hand, the Zr K-edge spectra (Fig. A.11) do not show any distinguishable shifts in the Zr edge energy. Fig. A.12 shows negligible differences in the Cu K-edge spectra of Cu-GaZrO_x-24 after 17 hours of ambient air exposure inside the hutch of the beamline.

3.3. CO₂ and H₂ adsorption

CO₂-TPD and CO₂ reaction order measurements were performed to gain insights on the catalysts ability to adsorb CO₂ and how that influences the rate of methanol production. The CO₂-TPD profiles (Fig. 5a) indicate that the Cu/Zr interface may play a role in CO₂ binding. The CO₂-TPD profile on the binary Cu-ZrO_x sample shows a broad low-temperature desorption peak around 75 °C and a sharp high-temperature one around 505 °C. The sharp high-temperature peak was not observed on the pure constituents Cu and ZrO₂ (Fig. A.13). The DSC curve for the CO₂-TPD on Cu-ZrO_x (Fig. A.14a) shows a sharp exothermic peak at 545 °C, slightly higher than the high desorption temperature of CO₂. Multiple CO₂-TPD experiments were run on this sample, but stopped at different temperatures: 500 °C, 600 °C, and 700 °C. The XRD patterns of the spent samples from these experiments were analyzed (Fig. A.14b). The sample treated to 500 °C was still amorphous. The samples treated at 600 °C and 700 °C showed crystalline peaks for t-ZrO₂ and metallic Cu. It follows that the exothermic DSC peak at 545 °C corresponds to the phase transformation from amorphous to crystalline, which may indicate that the amorphous nature of Cu-ZrO_x plays a role in its ability to adsorb appreciable amounts of the CO₂ species that require high temperatures to desorb. The addition of small amount of Ga to Cu-ZrO_x shifts the high-temperature CO₂ desorption peak to higher temperatures. However, the intensity of the high-temperature desorption peak decreases for the samples with high Ga content. The binary Cu-GaO_x adsorbed CO₂ the least. Nevertheless, the reaction order measurements (Fig. A.15) indicate negative reaction orders in CO₂ on all tested catalysts, including Cu-GaO_x ($n_{CO_2} = -0.2$). This result implies that: (i) adsorbed CO₂ poisons the sites involved in methanol formation and (ii) although Cu-GaO_x showed the least adsorbed CO₂ in its CO₂-TPD profile, that amount was still enough to inhibit the reaction and cause a negative order in CO₂. All this evidence indicates that the catalysts are likely to be limited by H₂, not CO₂.

To probe the ability of each sample to adsorb H₂ and how it affects

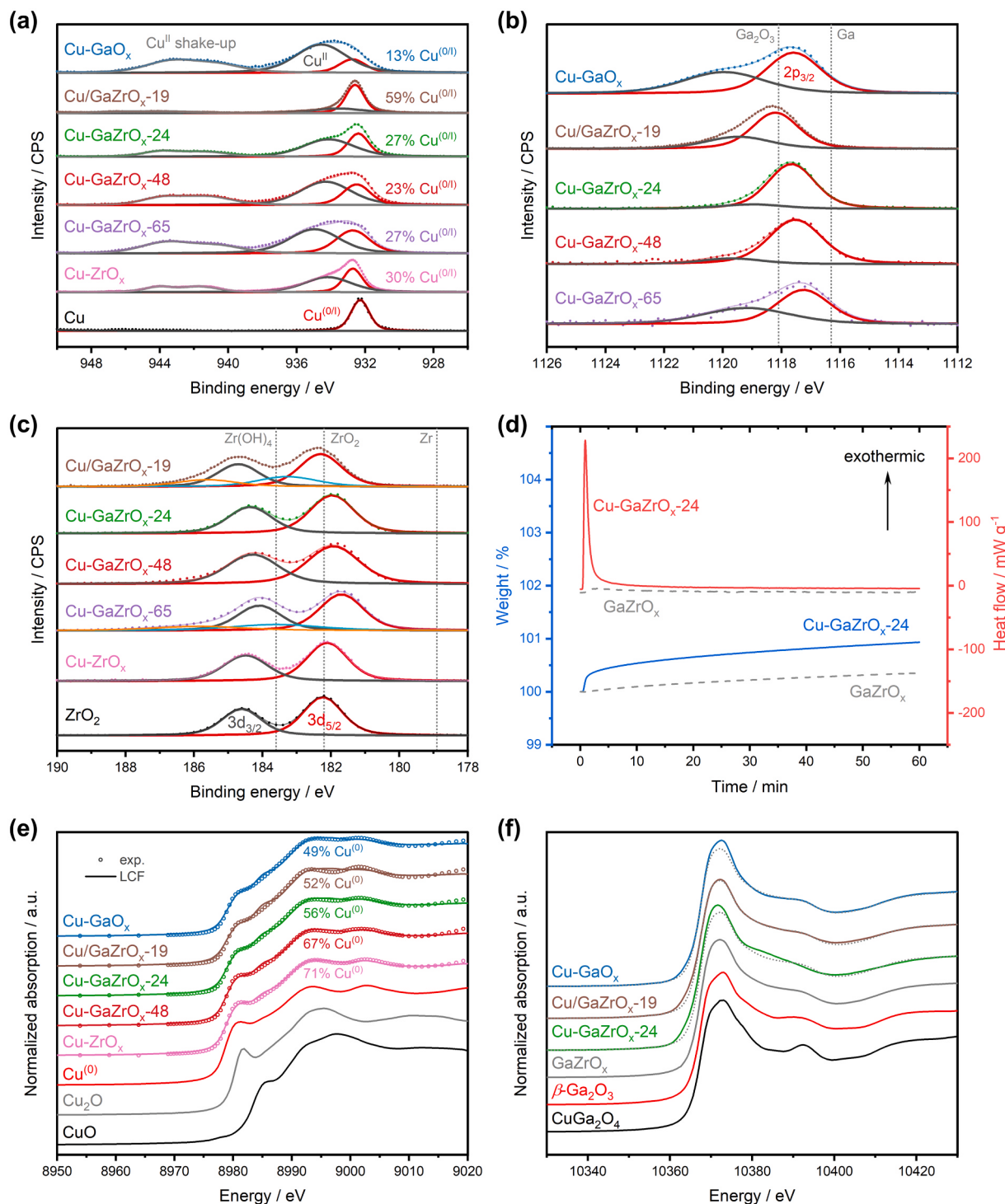


Fig. 4. (a) Cu 2p, (b) Ga 2p, and (c) Zr 3d XPS spectra of reduced CuGaZrO_x samples. (d) TGA-DSC profiles of introducing air at 30 °C over freshly reduced CuGaZrO_x-24 and GaZrO_x in 4% H₂/N₂ at 300 °C and cooled in N₂. (e) Cu K-edge and (f) Ga K-edge XAS spectra on reduced CuGaZrO_x samples. The reference dotted lines in (f) indicate the spectra corresponding to the GaZrO_x sample.

the rate of methanol production, H₂-TPD and H₂ reaction order measurements were performed. The H₂-TPD profiles (Fig. 5b) show that the Cu-GaO_x is the catalyst that adsorbs the most hydrogen. According to its H₂-TPD profile, there are two H₂ desorption peaks on Cu-GaO_x, one centered at 163 °C and the other centered at 361 °C. The H₂-TPD profile of Cu-GaZrO_x-24 was similar to that of Cu-GaO_x, but with slightly less intense peaks. The other samples (Cu/GaZrO_x-19, GaZrO_x, and Cu-ZrO_x) adsorbed far less H₂, which hints at the importance of the Cu/Ga interface for H₂ adsorption and stabilizing H species on the surface. Pure

Cu and Ga₂O₃ did not show the high H₂ adsorption capability of Cu-GaO_x (Fig. A.16). Impregnating Cu on GaZrO_x (Cu(IWI)/GaZrO_x-19) resulted in a sample that did not adsorb as much H₂ as the similar in composition Cu-GaZrO_x-24 sample, likely due to the lower Cu dispersion and low level of mixing between surface Cu and Ga in the IWI sample as shown by XPS. Representative H₂ reaction orders for methanol production on these catalysts are shown in Fig. A.17. The hydrogenation of CO₂ to methanol is first order in H₂ on Cu-ZrO_x and Cu-GaZrO_x-24. On the binary Cu-GaO_x, the H₂ reaction is less positive ($n(H_2) = 0.6$), which

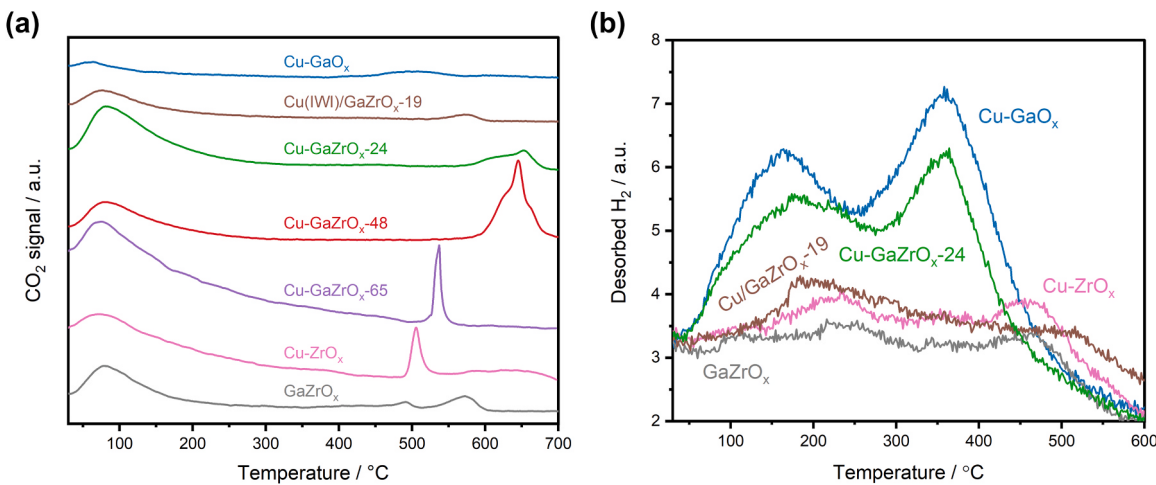


Fig. 5. (a) CO₂-TPD profiles of the CuGaZrO_x samples after reduction. The samples (50 mg each) were heated in N₂ with a ramp rate of 10 °C min⁻¹. (b) H₂-TPD profiles of the CuGaZrO_x samples after reduction. The samples (40 mg each) were heated in Ar with a ramp rate of 10 °C min⁻¹.

is consistent with this catalyst's superior ability to adsorb H₂ according to its H₂-TPD profile.

3.4. Mechanistic insights

Methanol formation is first order (or close to first order) in H₂ over CuGaZrO_x catalysts, suggesting that the breaking of H–H bonds (H₂ + 2* → 2 H^{*}, where an asterisk (*) denotes a free adsorption site and H^{*} denotes an adsorbed H species) is the rate limiting step. As a probe reaction to examine this hypothesis, H₂/D₂ exchange (H₂ + D₂ ⇌ 2HD) was performed using an equimolar feed of H₂ and D₂ [69]. The equilibrium conversion for this isotopic scrambling reaction is just above 47% at room temperature and gradually approaches 50% (binomial isotopologue distribution) at higher temperatures [70,71]. The exchange experiments were performed in a continuous flow reactor at 140 °C and 6 bar (20% H₂/20% D₂/Ar and 20% H₂/20% D₂/10% CO₂/Ar), keeping the catalyst mass and inlet flowrate constant. The exchange reaction temperature of 140 °C was set to: (i) achieve appreciable conversions at steady state (but still be far from thermodynamic equilibrium), (ii) limit side reactions from CO₂ hydrogenation in order to isolate the effect of CO₂ on poisoning the H₂/D₂ exchange sites without forming any products, and (iii) minimize the formation of weakly bound CO₂ species that were observed in the CO₂-TPD profiles (desorption peaks below 100 °C in Fig. 5a) and are unlikely to play a role during CO₂

hydrogenation (typically carried out between 200 and 300 °C). Fig. 6a shows that the best sample to catalyze the exchange reaction without CO₂ was Cu(IWI)/GaZrO_x-19 at 38% conversion. Its parent support, GaZrO_x, was the least active catalyst at just 13% exchange conversion. These results are in line with metallic Cu being the active site for H₂ activation. After the introduction of CO₂ ((H₂+D₂)/CO₂ = 4/1), the H₂ conversion dropped in all the catalysts by 4–9%, except for the IWI sample on which the conversion remarkably dropped by 20%. Based on the assumption that methanol production is rate limited by H₂ dissociation, the drop in the H₂/D₂ exchange conversion after the introduction of CO₂ is consistent with the methanol production being negative order in CO₂ on these catalysts. The remarkable drop in the Cu(IWI)-GaZrO_x-19 ability to exchange H₂/D₂ after the introduction of CO₂ further highlights that the synthesis method is an additional parameter that affects catalytic properties. Within the coprecipitated samples, the H₂/D₂ exchange ability largely followed the observed catalytic activity for the CO₂ hydrogenation reaction to methanol. In fact, Fig. 6b shows that there is a linear correlation between the H₂/D₂ exchange conversion and the methanol STY for the coprecipitated Cu-based catalysts. The linearity still holds when the regression includes the industrially relevant Cu/ZnO/Al₂O₃, a coprecipitated catalyst. It should be noted that the H₂/D₂ exchange on Cu/ZnO/Al₂O₃ without CO₂ in the feed may have been limited by equilibrium. Nevertheless, after the introduction of CO₂, the exchange conversion on Cu/ZnO/Al₂O₃ dropped to 31% and

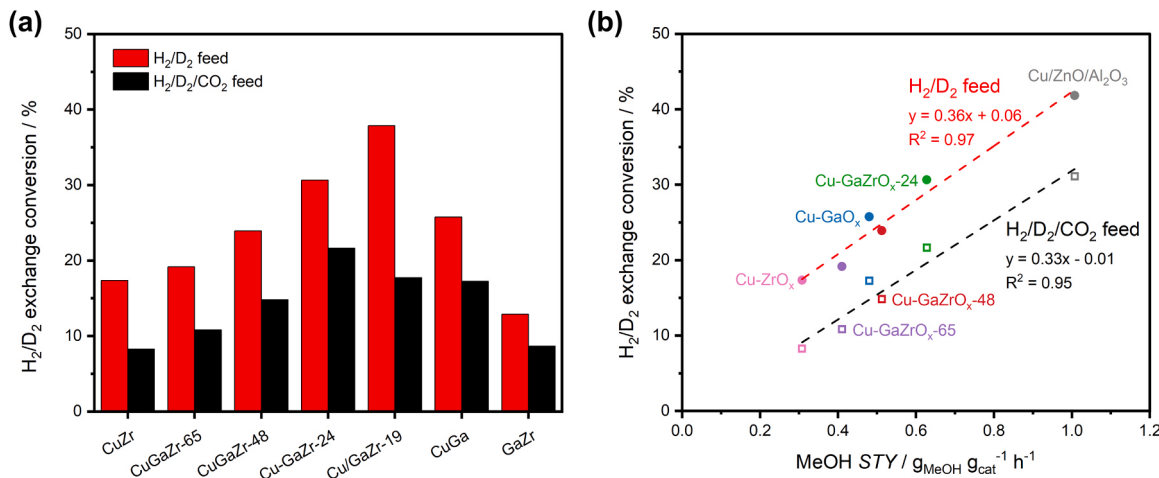


Fig. 6. (a) H₂/D₂ exchange conversion on CuGaZrO_x samples at 140 °C and 6 bar using inlet composition of (20% H₂/20% D₂/Ar) and (20% H₂/20% D₂/10% CO₂/Ar). (b) H₂/D₂ exchange conversion as a function of the methanol STY on the coprecipitated CuGaZrO_x samples as well as the industrial Cu/ZnO/Al₂O₃.

the linearity still holds. These results suggest that the H₂/D₂ exchange reaction serves as an appropriate descriptor for methanol STY on analogous CO₂ hydrogenation catalysts of similar syntheses. The linear correlations with and without CO₂ had similar slopes whereas the y-intercept had a value closer to zero after the introduction of CO₂.

Apparent activation energies were experimentally determined to investigate how composition affects the barriers to form methanol and CO (Fig. 7 and Fig. A.18). The methanol formation barriers were similar (between 36 and 41 kJ mol⁻¹) for all catalysts. However, the barrier to form CO was lower for low Ga content (< 5 wt% Ga) catalysts. Starting from Cu-GaZrO_x-48 (9 wt% Ga), the barrier to form CO increased by 28 kJ mol⁻¹ relative to the barrier on Cu-GaZrO_x-65 (4 wt% Ga). Increasing the Ga content further did not significantly influence the apparent activation energy to form CO. It could be suggested that the addition of a small amount of Ga suppresses the formation of CO. In this case, the high methanol selectivity on the samples with high Ga content is not because they form methanol more easily, but because they suppress the formation of CO. A possible reaction network for methanol and CO production that is consistent with our results is shown in Fig. 8. We propose that CO formation is possible directly from CO₂ with a higher energy barrier or indirectly through an intermediate with a lower energy barrier. The shared intermediate selectively turns into methanol with a low energy barrier on Ga-rich samples. Alternatively, the intermediate selectively decomposes to CO on Zr-rich samples. The proposed pathway is consistent with the ones reported in the literature, with the shared intermediate being a formate, methoxy, or carboxyl species [24,72–74].

4. Conclusions

We have synthesized, evaluated, and characterized ternary CO₂ hydrogenation catalysts containing Cu, Ga, and Zr at different Ga/Zr ratios. Our reactivity data show that the highest methanol STY occurs on a coprecipitated ternary catalyst, which outperforms the IWI counterpart and the constituent coprecipitated binaries (CuGaO_x, CuZrO_x, and GaZrO_x). In our efforts to systematically investigate the synergy between the metals in these catalysts, we discovered that the Cu/Zr interface plays a role in CO₂ adsorption while the Cu/Ga interface plays a role in H₂ adsorption. The methanol formation rate on these catalysts was found to be first order in H₂ and negative order in CO₂. We hypothesized that the dissociation of H–H bonds is the rate-limiting step for methanol formation. We showed that methanol STY is in fact linearly correlated to the H₂/D₂ exchange rate at 140 °C. Introducing CO₂ as part of the feed during the H₂/D₂ exchange experiments lowered the exchange conversion, but the effect of CO₂ was similar on all the catalysts of the same synthesis method. Therefore, the linear correlations between methanol STY and H₂/D₂ exchange rate with and without CO₂ have similar slopes, but different y-intercepts, which makes the H₂/D₂ exchange reaction a suitable descriptor for methanol STY. We also reported the apparent activation barriers for methanol and CO formation on these catalysts. The methanol formation barrier was similar on all the catalysts. However, as the Ga content increased, the barrier to form CO increased. Based on our results, we proposed a reaction network consisting of two routes for CO formation. The lower energy route to form CO shares an intermediate with methanol formation. We anticipate that our results and the provided methodology will help guide the design of effective heterogenous catalysts for CO₂ hydrogenation to methanol.

CRediT authorship contribution statement

Maria Fabregas-Angulo: Validation, Methodology, Investigation, Formal analysis, Data curation. **Yomaira Pagán-Torres:** Writing – review & editing, Writing – original draft, Visualization, Validation, Project administration, Methodology, Funding acquisition, Formal analysis. **Ryan Hagmann:** Formal analysis, Data curation. **Ive Hermans:** Writing – review & editing, Writing – original draft, Resources, Project administration, Methodology, Funding acquisition, Formal

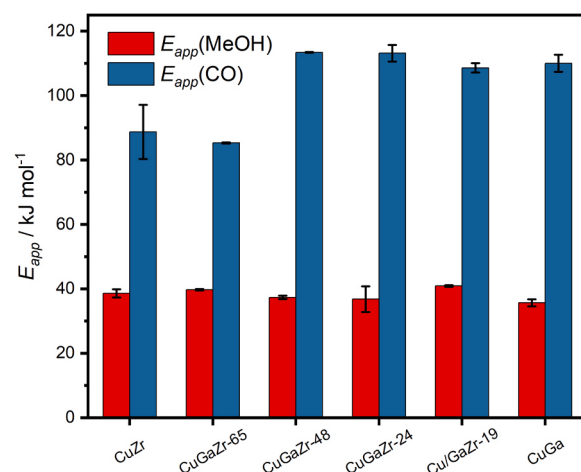


Fig. 7. Apparent activation barrier (E_{app}) of methanol and CO production on CuGaZrO_x catalysts. Reactor pressure was 35 bar, inlet H₂/CO₂ ratio was 4/1, and WHSV was 48,000 mL(STP) g_{cat}⁻¹ h⁻¹. Reactor temperature was varied between 220 and 280 °C.

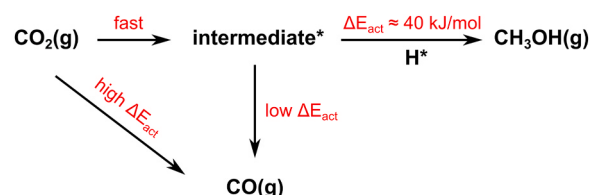


Fig. 8. Proposed CO₂ hydrogenation pathway to methanol and CO. An asterisk (*) denotes adsorbed species.

analysis. **Faysal Ibrahim:** Formal analysis, Data curation. **Jacob Jansen:** Formal analysis, Data curation. **Zhuoran Sun:** Data curation. **Edgar Turizo-Pinilla:** Investigation, Data curation. **Eranda Nikolla:** Supervision, Project administration, Investigation, Funding acquisition, Formal analysis, Conceptualization. **Collin Queen:** Data curation. **Abdullah Al Abdulghani:** Writing – review & editing, Writing – original draft, Visualization, Validation, Methodology, Investigation, Formal analysis, Data curation, Conceptualization. **Theodore Agbi:** Formal analysis, Data curation. **Samiha Bhat:** Visualization, Formal analysis, Data curation. **Miguel Sepúlveda-Pagán:** Data curation. **Morgan Kraimer:** Data curation.

Declaration of Competing Interest

The authors declare that they have no known competing financial interests or personal relationships that could have appeared to influence the work reported in this paper.

Data Availability

Data will be made available on request.

Acknowledgements

Support for this research was provided by the Office of the Vice Chancellor for Research and Graduate Education at the University of Wisconsin–Madison with funding from the Wisconsin Alumni Research Foundation. Support for this research was also provided by the National Science Foundation Partnership for Research and Education in Materials (PREM) Award DMR-1827894. S. Bhat and E. Nikolla acknowledge support from the United States National Science Foundation under Grant Number CBET2321164. This research used resources of the Advanced

Photon Source, a U.S. Department of Energy (DOE) Office of Science user facility operated for the DOE Office of Science by Argonne National Laboratory under Contract No. DE-AC02-06CH11357. The authors thank Sudipta Ganguly, Diana M. Aponte-Claudio, and Paola N. Fargas-López for their help in synthesizing the catalysts, Unni Kurumbail for providing scripts to analyze temperature programmed data, and Steve Myers and Dr. Blaise Thompson for their great assistance in building the TCD and MS setups used in this work. The authors also thank Dr. Sungsik Lee for the assistance with the XAS experiments at Argonne National Laboratory.

Appendix A. Supporting information

Supplementary data associated with this article can be found in the online version at doi:10.1016/j.apcatb.2024.124198.

References

- [1] A. González-Garay, M.S. Frei, A. Al-Qahtani, C. Mondelli, G. Guillén-Gosálbez, J. Pérez-Ramírez, Plant-to-planet analysis of CO₂-based methanol processes, *Energy Environ. Sci.* 12 (2019) 3425–3436, <https://doi.org/10.1039/C9EE01673B>.
- [2] T.P. Araújo, A. Shah, C. Mondelli, J.A. Stewart, D. Curulla Ferré, J. Pérez-Ramírez, Impact of hybrid CO₂-CO feeds on methanol synthesis over In2O3-based catalysts, *Appl. Catal. B Environ.* 285 (2021) 119878, <https://doi.org/10.1016/j.apcatb.2021.119878>.
- [3] V.A. Panchenko, Y.V. Daus, A.A. Kovalev, I.V. Yudaev, Y.V. Litti, Prospects for the production of green hydrogen: Review of countries with high potential, *Int. J. Hydrog. Energy* 48 (2023) 4551–4571, <https://doi.org/10.1016/j.ijhydene.2022.10.084>.
- [4] B.E. Lebrouhi, J.J. Djoupo, B. Lamrani, K. Benabdellaziz, T. Kouskou, Global hydrogen development - A technological and geopolitical overview, *Int. J. Hydrog. Energy* 47 (2022) 7016–7048, <https://doi.org/10.1016/j.ijhydene.2021.12.076>.
- [5] Q. Hassan, A.M. Abdulateef, S.A. Hafedh, A. Al-samari, J. Abdulateef, A.Z. Sameen, H.M. Salman, A.K. Al-Jibrooy, S. Wieteska, M. Jaszczerzak, Renewable energy-to-green hydrogen: A review of main resources routes, processes and evaluation, *Int. J. Hydrog. Energy* 48 (2023) 17383–17408, <https://doi.org/10.1016/j.ijhydene.2023.01.175>.
- [6] G.A. Olah, Towards oil independence through renewable methanol chemistry, *Angew. Chem. Int. Ed.* 52 (2013) 104–107, <https://doi.org/10.1002/anie.201204995>.
- [7] R.-P. Ye, J. Ding, W. Gong, M.D. Argyle, Q. Zhong, Y. Wang, C.K. Russell, Z. Xu, A. G. Russell, Q. Li, M. Fan, Y.-G. Yao, CO₂ hydrogenation to high-value products via heterogeneous catalysis, *Nat. Commun.* 10 (2019) 5698, <https://doi.org/10.1038/s41467-019-13638-9>.
- [8] W. Wang, C. Zeng, N. Tsubaki, Recent advancements and perspectives of the CO₂ hydrogenation reaction, *Green. Carbon* 1 (2023) 133–145, <https://doi.org/10.1016/j.greencarbon.2023.10.003>.
- [9] S. Kattel, P.J. Ramírez, J.G. Chen, J.A. Rodriguez, P. Liu, Active sites for CO₂ hydrogenation to methanol on Cu/ZnO catalysts, *Science* 355 (2017) 1296–1299, <https://doi.org/10.1126/science.aal3573>.
- [10] S. Kanuri, S. Roy, C. Chakraborty, S.P. Datta, S.A. Singh, S. Dinda, An insight of CO₂ hydrogenation to methanol synthesis: Thermodynamics, catalysts, operating parameters, and reaction mechanism, *Int. J. Energy Res.* 46 (2022) 5503–5522, <https://doi.org/10.1002/er.7562>.
- [11] G. Bonura, M. Cordaro, C. Cannilla, F. Arena, F. Frusteri, The changing nature of the active site of Cu-Zn-Zr catalysts for the CO₂ hydrogenation reaction to methanol, *Appl. Catal. B Environ.* 152–153 (2014) 152–161, <https://doi.org/10.1016/j.apcatb.2014.01.035>.
- [12] X. Cui, Y. Liu, W. Yan, Y. Xue, Y. Mei, J. Li, X. Gao, H. Zhang, S. Zhu, Y. Niu, T. Deng, Enhancing methanol selectivity of commercial Cu/ZnO/Al₂O₃ catalyst in CO₂ hydrogenation by surface silylation, *Appl. Catal. B Environ.* 339 (2023) 123099, <https://doi.org/10.1016/j.apcatb.2023.123099>.
- [13] B.C. Dharmalingam, A. Koushik V, M. Mureddu, L. Atzori, S. Lai, A. Pettinai, N. S. Kaisare, P. Aghalayam, J.J. Varghese, Unravelling the role of metal-metal oxide interfaces of Cu/ZnO/ZrO₂/Al₂O₃ catalyst for methanol synthesis from CO₂: insights from experiments and DFT-based microkinetic modeling, *Appl. Catal. B Environ.* 332 (2023) 122743, <https://doi.org/10.1016/j.apcatb.2023.122743>.
- [14] H. Zhang, D. Mao, J. Zhang, D. Wu, Tuning the CO₂ hydrogenation path by moderately phosphating the Co-Al catalyst toward methanol synthesis, *Appl. Catal. B Environ.* 340 (2024) 123257, <https://doi.org/10.1016/j.apcatb.2023.123257>.
- [15] J. Zhong, X. Yang, Z. Wu, B. Liang, Y. Huang, T. Zhang, State of the art and perspectives in heterogeneous catalysis of CO₂ hydrogenation to methanol, *Chem. Soc. Rev.* 49 (2020) 1385–1413, <https://doi.org/10.1039/C9CS00614A>.
- [16] H.-X. Li, L.-Q.-Q. Yang, Z.-Y. Chi, Y.-L. Zhang, X.-G. Li, Y.-L. He, T.R. Reina, W.-D. Xiao, CO₂ Hydrogenation to Methanol Over Cu/ZnO/Al₂O₃ Catalyst: Kinetic Modeling Based on Either Single- or Dual-Active Site Mechanism, *Catal. Lett.* 152 (2022) 3110–3124, <https://doi.org/10.1007/s10562-021-03913-0>.
- [17] Y. He, F.H. Müller, R. Palkovits, F. Zeng, C. Mebrahtu, Tandem catalysis for CO₂ conversion to higher alcohols: a review, *Appl. Catal. B Environ.* 345 (2024) 123663, <https://doi.org/10.1016/j.apcatb.2023.123663>.
- [18] A. Beck, M. Zabilskiy, M.A. Newton, O. Safonova, M.G. Willinger, J.A. van Bokhoven, Following the structure of copper-zinc-alumina across the pressure gap in carbon dioxide hydrogenation, *Nat. Catal.* 4 (2021) 488–497, <https://doi.org/10.1038/s41929-021-00625-x>.
- [19] Z. Zhang, S. Cheng, W. Liu, B. Chen, X. Gao, P. Wang, J. Gao, Y. Tan, S. Dang, W. Tu, Unraveling the regulation of Mn in Cu/ZnO formation during methanol synthesis from syngas over Cu/ZnO/Al₂O₃-Mn catalysts, *Appl. Catal. B Environ.* 338 (2023) 122985, <https://doi.org/10.1016/j.apcatb.2023.122985>.
- [20] M. Zabilskiy, V.L. Sushkevich, D. Palagin, M.A. Newton, F. Krumeich, J.A. van Bokhoven, The unique interplay between copper and zinc during catalytic carbon dioxide hydrogenation to methanol, *Nat. Commun.* 11 (2020) 2409, <https://doi.org/10.1038/s41467-020-16342-1>.
- [21] I. Kasatkin, P. Kurr, B. Kniep, A. Trunschke, R. Schlögl, Role of lattice strain and defects in copper particles on the activity of Cu/ZnO/Al₂O₃ catalysts for methanol synthesis, *Angew. Chem. Int. Ed.* 46 (2007) 7324–7327, <https://doi.org/10.1002/anie.200702600>.
- [22] M.S. Frei, F.L.P. Veenstra, D. Capeder, J.A. Stewart, D. Curulla-Ferré, A.J. Martín, C. Mondelli, J. Pérez-Ramírez, Microfabrication enables quantification of interfacial activity in thermal catalysis, *Small Methods* 5 (2021) 2001231, <https://doi.org/10.1002/smtd.202001231>.
- [23] X. Jiang, X. Nie, X. Guo, C. Song, J.G. Chen, Recent advances in carbon dioxide hydrogenation to methanol via heterogeneous catalysis, *Chem. Rev.* (2020), <https://doi.org/10.1021/acs.chemrev.9b00723>.
- [24] S. Kattel, P. Liu, J.G. Chen, Tuning selectivity of CO₂ hydrogenation reactions at the metal/oxide interface, *J. Am. Chem. Soc.* 139 (2017) 9739–9754, <https://doi.org/10.1021/jacs.7b05362>.
- [25] I. Abbas, H. Kim, C.-H. Shin, S. Yoon, K.-D. Jung, Differences in bifunctionality of ZnO and ZrO₂ in Cu/ZnO/ZrO₂/Al₂O₃ catalysts in hydrogenation of carbon oxides for methanol synthesis, *Appl. Catal. B Environ.* 258 (2019) 117971, <https://doi.org/10.1016/j.apcatb.2019.117971>.
- [26] K. Li, J.G. Chen, CO₂ Hydrogenation to methanol over ZrO₂-containing catalysts: insights into ZrO₂ induced synergy, *ACS Catal.* 9 (2019) 7840–7861, <https://doi.org/10.1021/acscatal.9b01943>.
- [27] B. Denise, O. Cherifi, M.M. Bettahar, R.P.A. Sneeden, Supported copper catalysts prepared from copper(II) formate: hydrogenation of carbon dioxide containing feedstocks, *Appl. Catal.* 48 (1989) 365–372, [https://doi.org/10.1016/S0166-9834\(00\)8205-5](https://doi.org/10.1016/S0166-9834(00)8205-5).
- [28] X. Chang, X. Zi, J. Li, F. Liu, X. Han, J. Chen, Z. Hao, H. Zhang, Z. Zhang, P. Gao, M. Li, J. Lv, X. Ma, An insight into synergistic metal-oxide interaction in CO₂ hydrogenation to methanol over Cu/ZnO/ZrO₂, *Catalysts* 13 (2023), <https://doi.org/10.3390/catal13101337>.
- [29] X. Dong, F. Li, N. Zhao, F. Xiao, J. Wang, Y. Tan, CO₂ hydrogenation to methanol over Cu/ZnO/ZrO₂ catalysts prepared by precipitation-reduction method, *Appl. Catal. B Environ.* 191 (2016) 8–17, <https://doi.org/10.1016/j.apcatb.2016.03.014>.
- [30] Y. Amenomiya, Methanol synthesis from CO₂ + H₂ II. Copper-based binary and ternary catalysts, *Appl. Catal.* 30 (1987) 57–68, [https://doi.org/10.1016/S0166-9834\(00\)81011-8](https://doi.org/10.1016/S0166-9834(00)81011-8).
- [31] M.S. Frei, C. Mondelli, A. Cesarin, F. Krumeich, R. Hauer, J.A. Stewart, D. Curulla Ferré, J. Pérez-Ramírez, Role of Zirconia in Indium Oxide-Catalyzed CO₂ Hydrogenation to Methanol, *ACS Catal.* 10 (2020) 1133–1145, <https://doi.org/10.1021/acscatal.9b03305>.
- [32] S. Tada, A. Katagiri, K. Kiyota, T. Honma, H. Kamei, A. Naruyuki, S. Uchida, S. Satokawa, Cu Species Incorporated into Amorphous ZrO₂ with High Activity and Selectivity in CO₂-to-Methanol Hydrogenation, *J. Phys. Chem. C* 122 (2018) 5430–5442, <https://doi.org/10.1021/acs.jpcc.7b11284>.
- [33] R.A. Koeppl, A. Baiker, A. Wokaun, Copper/zirconia catalysts for the synthesis of methanol from carbon dioxide: Influence of preparation variables on structural and catalytic properties of catalysts, *Appl. Catal. A Gen.* 84 (1992) 77–102, [https://doi.org/10.1016/0926-860X\(92\)80340-I](https://doi.org/10.1016/0926-860X(92)80340-I).
- [34] E. Lam, K. Larmier, S. Tada, P. Wolf, O.V. Safonova, C. Copérat, Zr(IV) surface sites determine CH₃OH formation rate on Cu/ZrO₂/SiO₂ - CO₂ hydrogenation catalysts, *Chin. J. Catal.* 40 (2019) 1741–1748, [https://doi.org/10.1016/S1872-0671\(19\)63348-6](https://doi.org/10.1016/S1872-0671(19)63348-6).
- [35] E. Lam, K. Larmier, P. Wolf, S. Tada, O.V. Safonova, C. Copérat, Isolated Zr Surface Sites on Silica Promote Hydrogenation of CO₂ to CH₃OH in Supported Cu Catalysts, *J. Am. Chem. Soc.* 140 (2018) 10530–10535, <https://doi.org/10.1021/jacs.8b05595>.
- [36] G. Noh, E. Lam, D.T. Bregante, J. Meyet, P. Šot, D.W. Flaherty, C. Copérat, Lewis Acid Strength of Interfacial Metal Sites Drives CH₃OH Selectivity and Formation Rates on Cu-Based CO₂ Hydrogenation Catalysts, *Angew. Chem. Int. Ed.* 60 (2021) 9650–9659, <https://doi.org/10.1002/anie.202010672>.
- [37] K. Larmier, W.-C. Liao, S. Tada, E. Lam, R. Verel, A. Bansode, A. Urakawa, A. Comas-Vives, C. Copérat, CO₂-to-Methanol Hydrogenation on Zirconia-Supported Copper Nanoparticles: Reaction Intermediates and the Role of the Metal-Support Interface, *Angew. Chem. Int. Ed.* 56 (2017) 2318–2323, <https://doi.org/10.1002/anie.201610166>.
- [38] R. Ladera, F.J. Pérez-Alonso, J.M. González-Carballo, M. Ojeda, S. Rojas, J.L. G. Fierro, Catalytic valorization of CO₂ via methanol synthesis with Ga-promoted Cu-ZnO-ZrO₂ catalysts, *Appl. Catal. B Environ.* 142–143 (2013) 241–248, <https://doi.org/10.1016/j.apcatb.2013.05.019>.
- [39] A.M. Hengne, D.J. Yuan, N.S. Date, Y. Saikh, S.P. Kamble, C.V. Rode, K.-W. Huang, Preparation and Activity of Copper–Gallium Nanocomposite Catalysts for Carbon Dioxide Hydrogenation to Methanol, *Ind. Eng. Chem. Res.* 58 (2019) 21331–21340, <https://doi.org/10.1021/acs.iecr.9b04083>.

- [40] E.L. Fornero, A.L. Bonivardi, M.A. Baltanás, Isotopic study of the rates of hydrogen provision vs. methanol synthesis from CO₂ over Cu–Ga–Zr catalysts, *J. Catal.* 330 (2015) 302–310, <https://doi.org/10.1016/j.jcat.2015.07.025>.
- [41] S.E. Collins, M.A. Baltanás, J.J. Delgado, A. Borgna, A.L. Bonivardi, CO₂ hydrogenation to methanol on Ga₂O₃-Pd/SiO₂ catalysts: Dual oxide-metal sites or (bi)metallic surface sites? *Catal. Today* 381 (2021) 154–162, <https://doi.org/10.1016/j.cattod.2020.07.048>.
- [42] J. Stoczyński, R. Grabowski, P. Olszewski, A. Kozłowska, J. Stoch, M. Lachowska, J. Skrzypek, Effect of metal oxide additives on the activity and stability of Cu/ZnO/ZrO₂ catalysts in the synthesis of methanol from CO₂ and H₂, *Appl. Catal. A Gen.* 310 (2006) 127–137, <https://doi.org/10.1016/j.apcata.2006.05.035>.
- [43] E. Lam, G. Noh, K.W. Chan, K. Larmier, D. Lebedev, K. Searles, P. Wolf, O. V. Safonova, C. Copéret, Enhanced CH₃OH selectivity in CO₂ hydrogenation using Cu-based catalysts generated via SOMC from GaII single-sites, *Chem. Sci.* 11 (2020) 7593–7598, <https://doi.org/10.1039/D0SC00465K>.
- [44] E.L. Fornero, P.B. Sanguineti, D.L. Chiavassa, A.L. Bonivardi, M.A. Baltanás, Performance of ternary Cu–Ga₂O₃–ZrO₂ catalysts in the synthesis of methanol using CO₂-rich gas mixtures, *Catal. Today* 213 (2013) 163–170, <https://doi.org/10.1016/j.cattod.2013.03.012>.
- [45] J.-Q. Zhong, S. Shaikhutdinov, B. Roldan Cuenya, Structural Evolution of Ga–Cu Model Catalysts for CO₂ Hydrogenation Reactions, *J. Phys. Chem. C* 125 (2021) 1361–1367, <https://doi.org/10.1021/acs.jpcc.0c09382>.
- [46] S.W. Lee, A. Subramanian, F.B. Zamudio, J.Q. Zhong, S.M. Kozlov, S. Shaikhutdinov, B. Roldan Cuenya, Interaction of Gallium with a Copper Surface: Surface Alloying and Formation of Ordered Structures, *J. Phys. Chem. C* 127 (2023) 20700–20709, <https://doi.org/10.1021/acs.jpcc.3c05711>.
- [47] P.B. Sanguineti, M.A. Baltanás, A.L. Bonivardi, Copper–gallia interaction in Cu–Ga₂O₃–ZrO₂ catalysts for methanol production from carbon oxide(s) hydrogenation, *Appl. Catal. A Gen.* 504 (2015) 476–481, <https://doi.org/10.1016/j.apcata.2014.11.021>.
- [48] W.-H. Feng, M.-M. Yu, L.-J. Wang, Y.-T. Miao, M. Shakouri, J. Ran, Y. Hu, Z. Li, R. Huang, Y.-L. Lu, D. Gao, J.-F. Wu, Insights into Bimetallic Oxide Synergy during Carbon Dioxide Hydrogenation to Methanol and Dimethyl Ether over GaZrOx Oxide Catalysts, *ACS Catal.* 11 (2021) 4704–4711, <https://doi.org/10.1021/acscatal.0c05410>.
- [49] M.C. Biesinger, L.W.M. Lau, A.R. Gerson, R.S.C. Smart, Resolving surface chemical states in XPS analysis of first row transition metals, oxides and hydroxides: Sc, Ti, V, Cu and Zn, *Appl. Surf. Sci.* 257 (2010) 887–898, <https://doi.org/10.1016/j.apsusc.2010.07.086>.
- [50] M.C. Biesinger, B.R. Hart, R. Polack, B.A. Kobe, R.S.C. Smart, Analysis of mineral surface chemistry in flotation separation using imaging XPS, *Miner. Eng.* 20 (2007) 152–162, <https://doi.org/10.1016/j.mineng.2006.08.006>.
- [51] M.C. Biesinger, Advanced analysis of copper X-ray photoelectron spectra, *Surf. Interface Anal.* 49 (2017) 1325–1334, <https://doi.org/10.1002/sia.6239>.
- [52] S. Sato, R. Takahashi, T. Sodesawa, K. Yuma, Y. Obata, Distinction between Surface and Bulk Oxidation of Cu through N₂O Decomposition, *J. Catal.* 196 (2000) 195–199, <https://doi.org/10.1006/jcat.2000.3028>.
- [53] A. Gervasini, S. Bennici, Dispersion and surface states of copper catalysts by temperature-programmed-reduction of oxidized surfaces (s-TPR), *Appl. Catal. A Gen.* 281 (2005) 199–205, <https://doi.org/10.1016/j.apcata.2004.11.030>.
- [54] K. Larmier, S. Tada, A. Comas-Vives, C. Copéret, Surface Sites in Cu-Nanoparticles: Chemical Reactivity or Microscopy? *J. Phys. Chem. Lett.* 7 (2016) 3259–3263, <https://doi.org/10.1021/acs.jpclett.6b01328>.
- [55] A. Dandekar, M.A. Vannice, Determination of the Dispersion and Surface Oxidation States of Supported Cu Catalysts, *J. Catal.* 178 (1998) 621–639, <https://doi.org/10.1006/jcat.1998.2190>.
- [56] R. Chatterjee, S. Kuld, R. van den Berg, A. Chen, W. Shen, J.M. Christensen, A. D. Jensen, J. Sehested, Mapping Support Interactions in Copper Catalysts, *Top. Catal.* 62 (2019) 649–659, <https://doi.org/10.1007/s11244-019-01150-9>.
- [57] O. Hinrichsen, T. Genger, M. Muhler, Chemisorption of N₂O and H₂ for the Surface Determination of Copper Catalysts, *Chem. Eng. Technol.* 23 (2000) 956–959, [https://doi.org/10.1002/1521-4125\(200011\)23:11<956::AID-CEAT956>3.0.CO;2-L](https://doi.org/10.1002/1521-4125(200011)23:11<956::AID-CEAT956>3.0.CO;2-L).
- [58] G.C. Chinchen, C.M. Hay, H.D. Vandervell, K.C. Waugh, The measurement of copper surface areas by reactive frontal chromatography, *J. Catal.* 103 (1987) 79–86, [https://doi.org/10.1016/0021-9517\(87\)90094-7](https://doi.org/10.1016/0021-9517(87)90094-7).
- [59] J.R. Jensen, T. Johannessen, H. Livbjerg, An improved N₂O-method for measuring Cu-dispersion, *Appl. Catal. A Gen.* 266 (2004) 117–122, <https://doi.org/10.1016/j.apcata.2004.02.009>.
- [60] J. Schumann, M. Eichelbaum, T. Lunkenbein, N. Thomas, M.C. Álvarez Galván, R. Schlögl, M. Behrens, Promoting Strong Metal Support Interaction: Doping ZnO for Enhanced Activity of Cu/ZnO:M (M = Al, Ga, Mg) Catalysts, *ACS Catal.* 5 (2015) 3260–3270, <https://doi.org/10.1021/acscatal.5b00188>.
- [61] Z. Wang, Z. Niu, Q. Hao, L. Ban, H. Li, Y. Zhao, Z. Jiang, Enhancing the Ethynylation Performance of CuO-Bi₂O₃ Nanocatalysts by Tuning Cu-Bi Interactions and Phase Structures, *Catalysts* 9 (2019), <https://doi.org/10.3390/catal9010035>.
- [62] G. Schön, Auger and direct electron spectra in X-ray photoelectron studies of zinc, zinc oxide, gallium and gallium oxide, *J. Electron Spectros. Relat. Phenom.* 2 (1973) 75–86, [https://doi.org/10.1016/0368-2048\(73\)80049-0](https://doi.org/10.1016/0368-2048(73)80049-0).
- [63] C.L. Hinkle, M. Milojevic, B. Brennan, A.M. Sonnet, F.S. Aguirre-Tostado, G. J. Hughes, E.M. Vogel, R.M. Wallace, Detection of Ga suboxides and their impact on III-V passivation and Fermi-level pinning, *Appl. Phys. Lett.* 94 (2009) 162101, <https://doi.org/10.1063/1.3120546>.
- [64] Y. Zheng, M. Fan, K. Li, R. Zhang, X. Li, L. Zhang, Z.-A. Qiao, Ultraviolet-induced Ostwald ripening strategy towards a mesoporous Ga₂O₃/GaOOH heterojunction composite with a controllable structure for enhanced photocatalytic hydrogen evolution, *Catal. Sci. Technol.* 10 (2020) 2882–2892, <https://doi.org/10.1039/D0CY00303D>.
- [65] L. Yang, X. Zhao, S. Xu, Y. Lu, H. Chang, J. Liu, Oxide transformation and break-up of liquid metal in boiling solutions, *Sci. China Technol. Sci.* 63 (2020) 289–296, <https://doi.org/10.1007/s11431-018-9444-5>.
- [66] M.I. Dar, S. Sampath, S.A. Shivashankar, Exploiting oriented attachment in stabilizing La³⁺-doped gallium oxide nano-spindles, *RSC Adv.* 4 (2014) 49360–49366, <https://doi.org/10.1039/C4RA07089E>.
- [67] G. Greczynski, L. Hultman, Towards reliable X-ray photoelectron spectroscopy: Sputter-damage effects in transition metal borides, carbides, nitrides, and oxides, *Appl. Surf. Sci.* 542 (2021) 148599, <https://doi.org/10.1016/j.apsusc.2020.148599>.
- [68] T.L. Barr, An ESCA study of the termination of the passivation of elemental metals, *J. Phys. Chem.* 82 (1978) 1801–1810, <https://doi.org/10.1021/J100505a006>.
- [69] C. Tang, S. Tang, F. Sha, Z. Han, Z. Feng, J. Wang, C. Li, Insights into the Selectivity Determinant and Rate-Determining Step of CO₂ Hydrogenation to Methanol, *J. Phys. Chem. C* 126 (2022) 10399–10407, <https://doi.org/10.1021/acs.jpcc.2c02995>.
- [70] S.L. Leung, D. Hibbitts, M. García-Díéguez, E. Iglesia, Binding and exchange reactions of hydrogen isotopes on surfaces of dispersed Pt nanoparticles, *J. Phys. Chem. C* 126 (2022) 3923–3938, <https://doi.org/10.1021/acs.jpcc.1c09131>.
- [71] D. Rittenberg, W. Bleakney, H.C. Urey, The equilibrium between the three hydrogens, *J. Chem. Phys.* 2 (2004) 48–49, <https://doi.org/10.1063/1.1749360>.
- [72] A. Bavykina, I. Yarulina, A.J. Al Abdulghani, L. Gevers, M.N. Hedhili, X. Miao, A. R. Galilea, A. Pustovarenko, A. Dikhtarenko, A. Cadiau, A. Aguilar-Tapia, J.-L. Hazemann, S.M. Kozlov, S. Oud-Chikh, L. Cavallo, J. Gascon, Turning a Methanation Co-Catalyst into an In–Co Methanol Producer, *ACS Catal.* 9 (2019) 6910–6918, <https://doi.org/10.1021/acscatal.9b01638>.
- [73] N.J. Azhari, D. Erika, S. Mardiana, T. Ilmi, M.L. Gunawan, I.G.B.N. Makertiharta, G.T.M. Kadja, Methanol synthesis from CO₂: A mechanistic overview, *Results Eng.* 16 (2022) 100711, <https://doi.org/10.1016/j.rineng.2022.100711>.
- [74] K. Wang, S. Shao, Y. Liu, M. Cao, J. Yu, C.H. Lau, Y. Zheng, X. Fan, DRIFTS-SSITKA-MS investigations on the mechanism of plasmon preferentially enhanced CO₂ hydrogenation over Au/γ-Al₂O₃, *Appl. Catal. B Environ.* 328 (2023) 122531, <https://doi.org/10.1016/j.apcatb.2023.122531>.